nature neuroscience

Precise olfactory responses tile the sniff cycle

Roman Shusterman[1], Matthew C Smear[1,2], Alexei A Koulakov[3] & Dmitry Rinberg[1]

In terrestrial vertebrates, sniffing controls odorant access to receptors, and therefore sets the timescale of olfactory stimuli. We found that odorants evoked precisely sniff-locked activity in mitral/tufted cells in the olfactory bulb of awake mouse. The trial-to-trial response jitter averaged 12 ms, a precision comparable to other sensory systems. Individual cells expressed odor-specific temporal patterns of activity and, across the population, onset times tiled the duration of the sniff cycle. Responses were more tightly time-locked to the sniff phase than to the time after inhalation onset. The spikes of single neurons carried sufficient information to discriminate odors. In addition, precise locking to sniff phase may facilitate ensemble coding by making synchrony relationships across neurons robust to variation in sniff rate. The temporal specificity of mitral/tufted cell output provides a potentially rich source of information for downstream olfactory areas.

Sensory systems must capture time-varying features of the external world. Several sensory systems respond to rapid stimulus dynamics with millisecond precision[1–4], which may be essential for information transmission[5]. Does olfaction employ similar principles to transmit information about odors to the brain? Compared with stimuli in other modalities, odorants have relatively slow kinetics, but, in many species, odor responses have temporal structure on a faster timescale, which may encode information about odor stimuli[6].

In air-breathing vertebrates, odor stimuli are partitioned by sniffing. Numerous lines of evidence suggest that olfactory neurons may encode information about odor not only by how many spikes they fire per sniff cycle, but also by the timing of those spikes in each sniff[7–9] (for a review, see ref. 10). For some olfactory discriminations, one sniff suffices for accurate perceptual decisions[11–13], thus constraining the time window of relevant processing. Inhalations are brief (50–150 ms), which suggests that coding is precisely and reliably timed.

To investigate information coding in olfaction, we studied how sniffing shapes the responses of mitral/tufted cells in awake mice. To address this question, we performed extracellular recording of mitral/tufted cell activity while simultaneously monitoring sniffing. For better stimulus control, we employed a head-fixed setup in which the animal's nose was in a constant position relative to the odor plume.

RESULTS

Modulation of odor responses by breathing cycle

We recorded mitral/tufted cell activity (7 mice, 66 cells) and sniffing in awake, head-restrained mice in response to passive odor delivery (467 cell-odor pairs) (**Fig. 1** and Online Methods). Sniffing was measured by intranasal pressure cannula (**Fig. 1a**,**b**). In the pressure signal, inhalation was indicated by negative pressure and exhalation by positive pressure (**Supplementary Figs. 1** and **2**). The average cycle duration was 358 ± 131 ms (s.d.; **Supplementary Table 1**). When spikes were aligned to odor onset, mitral/tufted cells appeared to show sparse responses (**Fig. 1c**,**d**)[14–17]. However, alignment of responses to odor stimulus onset ignores a fundamental fact: the animal's sniffing controls access of odorants to olfactory receptor neurons[18]. Aligning mitral/tufted cell responses to the onset of the first inhalation after odor onset revealed strong and temporally precise odor responses (**Fig. 1c**,**d**). Many odorant responses consist of sharp peaks in activity, during which the firing rate may increase by several-fold above baseline. These peaks are often tightly locked to the sniff rhythm, reliably occurring at a particular latency after inhalation onset. Because these events can consist of a few spikes per trial, they can be seen only when the information about inhalation timing is used.

In the awake mouse, sniff cycles vary in duration, amplitude and waveform (**Supplementary Fig. 2**). As a result of this natural variability, the time course of receptor stimulation desynchronizes from trial to trial. Thus, aligning different trials only by inhalation onset may fail to capture the neuronal dynamics across multiple trials. To compare neuronal responses across trials, we stretched or compressed individual sniffs to a common standard. We defined two intervals: the inhalation phase and the remainder of the sniffing cycle, including exhalation (**Fig. 1b** and **Supplementary Fig. 2**). Across multiple animals and sessions, the average duration of the inhalation interval was 111 ± 44 ms and of exhalation is 247 ± 113 ms (see **Supplementary Table 1**). We morphed the first and second intervals of each sniff so that their durations became equal to these average values. Corresponding spike trains were morphed accordingly. This warping procedure transformed real-time coordinates into sniff phase coordinates (**Fig. 1c**,**d**)[8,19], which we refer to as sniff-warped time.

Analysis of mitral/tufted cell responses in sniff-warped coordinates uncovered temporal structure that was not evident from alignment to inhalation onset alone (**Fig. 1c**,**d**). First, sniffing modulated the firing rate even in the absence of odor stimuli (**Supplementary Fig. 3**). Second, after odor onset, the firing rate peak was higher and sharper in warped time coordinates for 71 of 78 cases (mean difference was 25 ± 22.9 Hz). Thus, aligning mitral/tufted cell spikes to the time course of sniffing unmasks precise temporal structure in odor responses.

[1]Janelia Farm Research Campus, Howard Hughes Medical Institute, Ashburn, Virginia, USA. [2]Department of Neurobiology and Physiology, Northwestern University, Evanston, Illinois, USA. [3]Cold Spring Harbor Laboratory, Cold Spring Harbor, New York, USA. Correspondence should be addressed to D.R. (rinbergd@janelia.hhmi.org).

Received 24 February; accepted 2 June; published online 17 July 2011; doi:10.1038/nn.2877

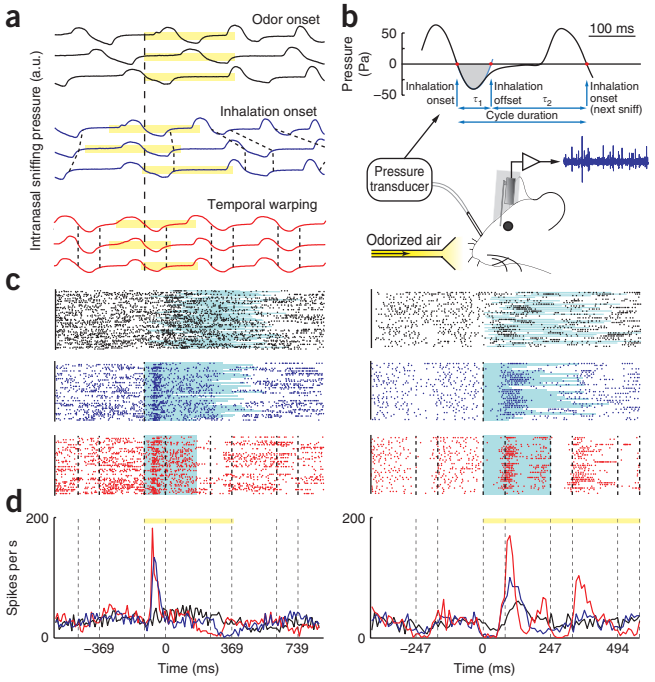

Figure 1 Odor response analysis: sniff-alignment and warping. (**a**) Intranasal pressure signal for three trials: aligned by odor onset (black), by the first inhalation after odor onset (blue) and temporally warped, so that each inhalation interval and the reminder of the sniff duration are equal to the average values (red). Yellow bars indicate the stimulus duration. Dashed lines indicate the beginning and the end of the inhalation intervals. (**b**) Schematic of the experiment. A head-fixed mouse was positioned in front of the odor delivery port. It was implanted with intranasal cannula and a multi-electrode chamber. Top, pressure waveform of a typical breathing cycle. Red dots indicate the inhalation onsets and offsets. The blue line is the parabolic fit to the first minimum after the inhalation onset. The sniff offset was defined as the second zero crossing of the parabolic fit. The gray shaded area marks the inhalation interval. (**c**,**d**) Raster and PSTH plots for two mitral/tufted cells (left and right columns) in response to an odor stimulus: synchronized by odor onset (black), inhalation onset (blue) and temporally warped (red). The light blue lines underlying the raster plots indicate the duration of the first sniff after odor onset. Vertical dashed lines indicate the beginning and end of inhalation intervals. Yellow bars indicate the odor stimulus duration.

Odor responses tile the sniff cycle

Response time courses were highly diverse across both cells and odors (**Fig. 2**). The temporal structure of responses was odor specific. For a single cell, different odors were able to evoke excitatory or inhibitory responses with different latencies and durations (**Fig. 2a**). All of the cells in our sample had nonzero baseline firing rates (16.2 ± 8.0 Hz), and a majority were modulated by sniffs in the absence of odor stimulus (**Supplementary Fig. 3**), consistent with what has been previously reported in awake rats[20].

One odorant could evoke diverse responses across cells (**Fig. 2b**). Cells differed in response sign and temporal pattern. Thus, a given odor evokes a heterogeneous set of firing events among mitral/tufted cells (**Fig. 2b**).

Across the population, sniff alignment and sniff warping revealed that responses were quite common among mitral/tufted cells. We scored a cell as being responsive to a given odorant if its cumulative spike count during odor presentation differed from its cumulative spike count without odor at one or more time points (**Fig. 3a–c** and Online Methods). Of the 467 cell-odor pairs, 275 (59%) displayed odor responses in the first sniff; 136 (29%) showed initially excitatory (**Fig. 3a**) and 139 (30%) showed initially inhibitory responses (**Fig. 3b**,**c**). Later in the cycle, some temporal response patterns changed sign from excitatory to inhibitory or vice versa. Of the 139 initially inhibitory responses, 27 became excitatory later in the sniffing cycle (**Fig. 3c**; see **Supplementary Table 2**).

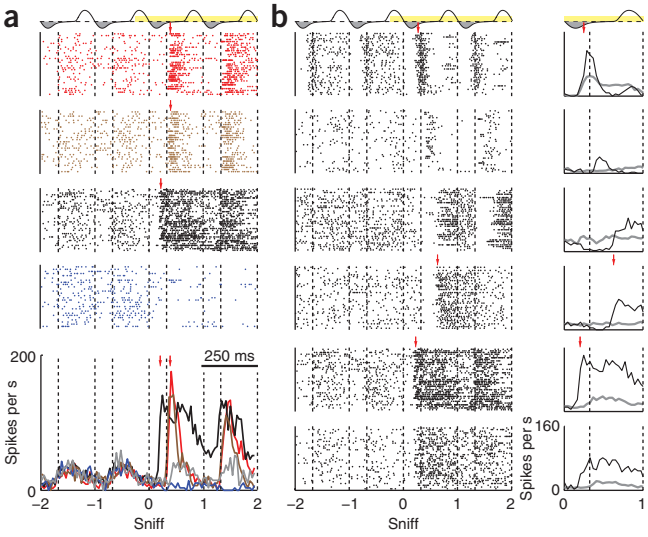

As a result of this multimodal patterning, some responses do not vary relative to background in the total number of spikes per sniff, but instead only vary in the phase of spikes in the sniff cycle[8]. We found that 19% of excitatory and 30% of inhibitory responses had the same total number of spikes during the first sniffing cycle (**Fig. 3d**,**e**). These cell-odor pairs, which had the same number of spikes per sniff with and without odor, most probably would not be counted as being odor responsive without synchronization with inhalation onset. In summary, 44% of cell-odor pairs had significant responses on the basis of first sniff spike count (Online Methods), and the percentage rose to 59% when precise timing was taken into account.

To determine whether odor responses tile the sniff cycle, we plotted sniff-warped, color-coded peristimulus time histograms (PSTHs) for all cell-odor pairs with significant excitatory or inhibitory responses (**Fig. 3d**,**e**). We subtracted spontaneous activity, here defined as the sniff-warped PSTH from unstimulated sniffs. We ordered the responses by latency, which is defined as the first time at which our statistical criterion was met. This rich diversity of response timings could strongly contribute to olfactory coding if the timings are sufficiently precise from trial to trial.

Responses are more precise in sniff phase coordinates

How precise is odor response timing? The relatively high spontaneous firing rate of mitral/tufted cells (16.2 ± 8.0 Hz) constrains the available methods for quantifying temporal precision. Thus, we focused our analysis on a subset of cell-odor pairs with a large increase in

Figure 2 Diversity of odor responses. (**a**) Sniff-warped raster plots and corresponding PSTHs of one cell's response to four odors: amyl acetate (red), benzaldehyde (black), hexanoic acid (brown) and methyl salicylate (blue). Response to blank is shown only on PSTH plot (gray). (**b**) Left, sniff-warped raster plots showing responses of six cells to the same odor (benzaldehyde). The stimulus interval is shown as a yellow bar above the plots. The sniff waveforms are shown above the plots and gray areas indicate inhalation intervals. Right, corresponding PSTH during the first sniff after odor onset (thin black line) and PSTH for unodorized sniffs (thick gray line). Vertical dashed lines indicate the beginning and end of inhalation. Red arrows indicate sharp event of firing rate increase.

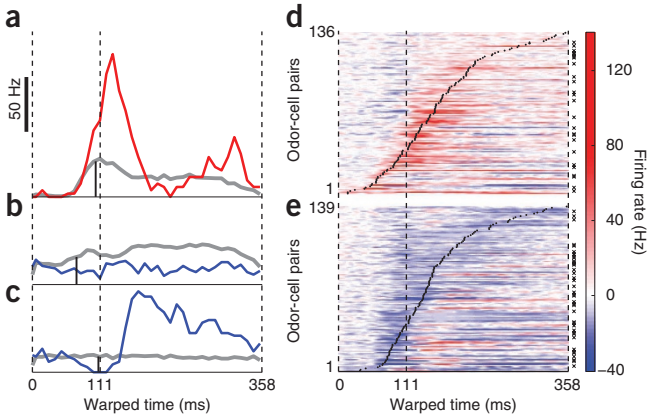

Figure 3 Excitatory and inhibitory odor responses tile the sniff cycle. (**a**–**c**) Examples of common types of odor response PSTHs: initially excitatory (**a**), initially inhibitory (**b**) and initially inhibitory switching to excitatory later in the sniffing cycle (**c**). The gray lines are PSTHs from unodorized sniffs. The black lines indicate response latency (τ_{lat}), defined as the first moment when cumulative distributions with and without stimulus become statistically different. (**d**,**e**) Color plot of all excitatory (**d**) and all inhibitory (**e**) responses. Each horizontal line represents the difference in spike histograms between odorized and unodorized sniffs for one cell-odor pair. The cell-odor pairs are ordered by response latency marked by black dots. The black crosses on the right of the color plot mark cell-odor pairs for which full sniff spike counts did not significantly differ between odorized and unodorized sniffs.

firing rate above baseline, hereafter referred to as sharp events (**Fig. 4** and Online Methods). Of these, 78 cell-odor pairs met our criterion for sharp events. To quantify precision, we determined the time of the first spike followed by an interspike interval below a criterion value[1] (**Fig. 4b**). For these sharp events, we defined latency as the across-trial mean of these first spike times. We quantified the precision of a sharp event by its jitter, that is, the s.d. of these first spike times across multiple trials. We defined a sharp event's reliability as the fraction of trials in which this interspike interval criterion was met (**Fig. 5**). We plotted sniff-warped PSTHs for all cell-odor pairs with sharp events, ordered by latency (**Fig. 4c**). The latencies tiled the whole inhalation interval and the beginning of the exhalation interval (**Fig. 4d**).

Temporal warping transforms the real time coordinates of spike trains to sniff phase time coordinates. How much does the temporal structure of mitral/tufted cell responses depend on our choice of time coordinates? We compared the precision distributions for all sharp events in sniff-warped and unwarped time coordinates (**Fig. 5a**). Without warping, the jitter was distributed broadly (mean, 23.7; median, 22.9 ms), whereas the jitter distribution tightened toward lower values in sniff-warped time coordinates (median, 10.5 ms; mean, 12.5; Kolmogorov-Smirnov test, $P = 4.6 \times 10^{-8}$). As another comparison, we plotted peak firing rates computed in both time coordinates (**Fig. 5b**). The majority of sharp-event firing-rate amplitudes were higher in the warped-time domain than in the real-time domain. Thus, by both measures, almost all sharp events were more precise in sniff-warped coordinates, suggesting that mitral/tufted cells encode information in sniff phase rather than real time.

Sniff-phase coding further predicts that jitter should co-vary with inhalation duration. To test this prediction, we selected the same cell-odor pairs with sharp events, split their trials into shortest and longest halves in terms of inhalation duration, and compared timing jitters across the two groups in real time. The jitter was smaller for fast inhalations (F test of distributions of jitters for long and short inhalations, $P = 6.1 \times 10^{-3}$), as evidenced by the preponderance of positive slopes (t test on slope distributions, $P = 1.3 \times 10^{-3}$; **Fig. 5d**). Consistent with sniff-phase coding, firing events became more precisely timed for shorter inhalations.

Odor information is transmitted on fast timescales

The refined temporal precision of odor responses (**Fig. 4c**) suggests that mitral cell activity carries information about odor at subsniff timescales. To measure this information, we evaluated the accuracy with which odorants can be discriminated on the basis of the mitral cell responses, on a trial-by-trial basis. If a mitral cell's firing carries a large amount of information about odorants, it will be highly predictive of the stimulus. To discriminate odorants from single trial responses, we used the template matching algorithm (TMA)[21]. This analysis enabled us to evaluate both robustness and temporal dynamics of olfactory information carried by the mitral cells (see Online Methods).

How well can a single neuron discriminate between two odor stimuli on the basis of a single trial? We applied TMA to all possible odor pairs for all neurons in warped time (1,734 cell-odor-odor combinations; **Fig. 6**). TMA was performed on concatenated bin vectors of firing rates with 5-ms bin size. Discrimination performance rose with the divergence of the PSTHs in response to the two odors (see example neurons in **Fig. 6a**). To quantify the temporal dependence of discrimination performance, we fit the rise in discrimination with a sigmoid function with three parameters: τ, the latency of transition, δ, the width of the transition, which characterizes the rise time of information accumulation, and D, the maximal discrimination success. Single neurons were able to discriminate odorants with high accuracy.

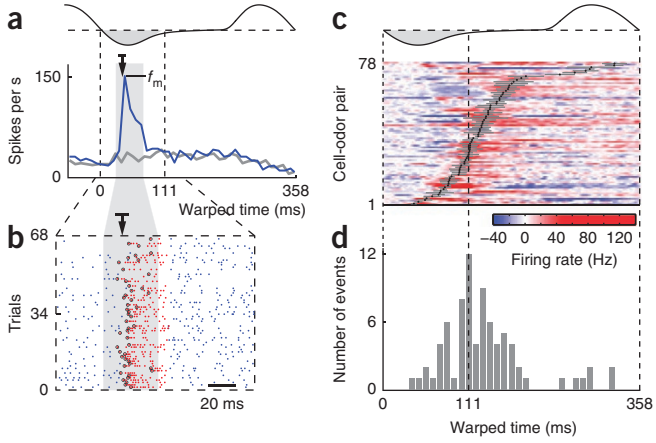

Figure 4 Sharp events of firing rate increase. (**a**) PSTHs of odor response (blue line) and spontaneous activity (gray line) in warped time for one cell-odor pair, 10-ms bin. f_m is the amplitude of the firing rate peak. (**b**) Zoomed raster plot of a sharp firing rate increase event. The gray area shows the interval around the peak of PSTH where sharp event is defined: from $-2/f_m$ to $+4/f_m$. The red dots are spikes with inter-spike interval less than $1.5/f_m$. The first of these spikes in a trial is colored black. The mean and s.d. of these first spikes define the sharp event's latency (indicated by black arrows) and precision (horizontal bars above arrows), respectively. (**c**) Color plot for cell-odor pairs with sharp events of differences between odor response and spontaneous activity firing rates for all cell odor pairs for which sharp events were detected, ordered by latency (black dots) in warped time coordinates. Gray bars around black dots show the s.d. (precision) of each sharp event. (**d**) Distribution of latencies for all sharp events in the same coordinates as **c**. Waveforms above **a** and **c** show the typical sniffing signal.

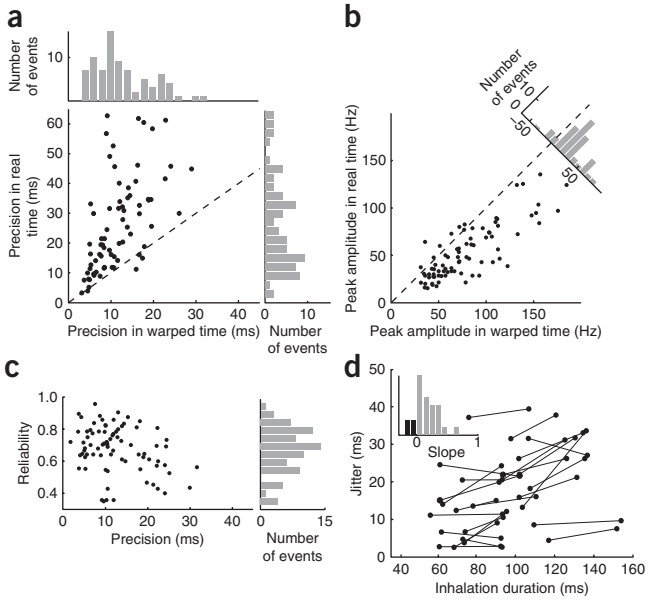

Figure 5 Mitral cell response precision in warped-time and real-time coordinates. (**a**) Scatter plot comparing precision of sharp events estimated in real time and warped time. Adjacent panels are distributions of precisions in warped and real time. (**b**) Scatter plot comparing firing rate peak amplitudes in warped and real time. Adjacent panel is the distribution of differences of the amplitudes in real and warped time. (**c**) Scatter plot of reliability of events versus precision of these events in warped time. Right, the distribution of reliabilities of the events. (**d**) Comparison of sharp event precision in real time domain for slow and fast inhalations. All sessions, which have more than 30 trials with detected sharp events, were split into two halves by the duration of the inhalation intervals. Pairs of connected dots are average jitters and inhalation durations for fast and slow inhalation intervals for individual sessions. Inset, distribution of slopes of the connecting lines.

This level of accuracy approaches the performance of animals in two-alternative tasks on a comparable timescale[11–13]. Furthermore, a mitral cell's information about odorants can emerge quite quickly, that is, the transition between the chance level and maximum performance can occur rapidly (for the example in **Fig. 6a**, $\delta = 8$ ms).

We found that 835 of 1,734 cell-odor-odor combinations had discrimination success above chance level (see Online Methods). The mean and median of the rise-time distribution were 104 and 75 ms, respectively; that of the discrimination-success distribution was 0.63 and 0.60, respectively (**Fig. 6b**). For some cell-odor-odor combinations, discrimination rose from chance level to maximal level ($D \approx 0.9$) in 10 ms (**Fig. 6b**). These fast transitions followed from the high temporal precision and reliability of the odor responses. We plotted the time courses of discrimination success for all above-chance cell-odor-odor combinations by the latency of the transition (**Fig. 6c**). Latencies of the transitions tiled the whole sniff cycle, similar to the odor responses.

Discrimination performance of neuronal populations

We next investigated the information contained in responses of populations of neurons. For five odors, the discrimination success of 25 neurons was 91% (TMA was performed on concatenated 30-ms time bins covering the whole sniff cycle). Decreasing the number of neurons from 25 to 5 lowered the discrimination success from 91% to 57% (**Fig. 7a**). However, if the best five discriminators were used for the given set of smells rather than using random sets of neurons, the performance went up to 84%. Discrimination success depended on which neurons were included in the pool. For a given number of neurons, the best discriminators outperformed randomly chosen neurons (**Fig. 7a**). The five best neurons performed only slightly worse (84%) than all 25 neurons (91%).

The best five neurons performed noticeably better than a random subset of five neurons. The maximum level of discrimination success was larger and the rate of growth was faster for the best five neurons (**Fig. 7b**). At the same time, both in the case of random and best subsets, the discrimination continued to improve throughout the sniff cycle. This feature was in contrast with the single-cell discrimination (**Fig. 6a**) and could be explained by tiling of the sniff cycle by the individual cells (**Fig. 6c**).

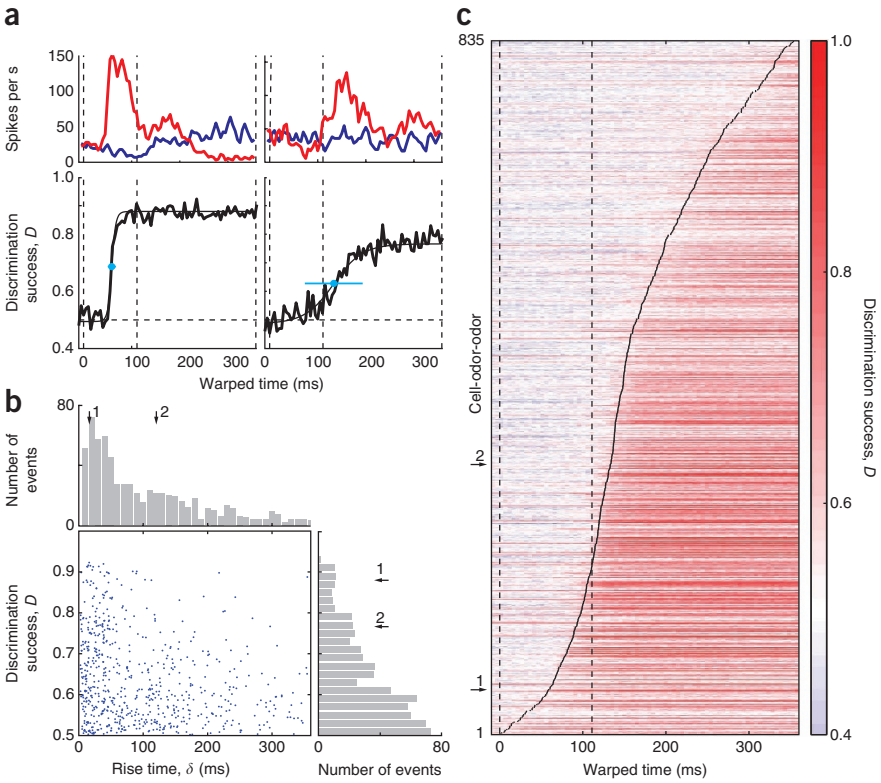

Figure 6 Discrimination performance of individual neurons. (**a**) Top, sniff-warped PSTHs for two neurons' responses to two odors each. Bottom, corresponding two-odor discrimination success as a function of sniff-warped time. Bin size is 5 ms in warped time. Vertical dashed lines indicate the beginning and the end of the inhalation interval and whole sniff cycle. The horizontal dashed line is chance level performance. The thin black line is a sigmoidal fit, which yields the latency of the transition, τ, the rise time of the transition, δ, and the maximal discrimination success, D (left: $\tau = 59$ ms, $\delta = 8$ ms, $D = 0.88$; right, $\tau = 133$ ms, $\delta = 60$ ms, $D = 0.77$). Blue dots and bars show the latencies and the widths of the transitions. (**b**) Scatter plot of rise time, δ, versus amplitude, D, for the 835 cell-odor-odor combinations. Distributions of δ and D are in the top and right panels, respectively. (**c**) Color plot of the time course of discrimination performance for 835 cell-odor-odor combinations, ordered by the latency of the transition, τ (black dots).

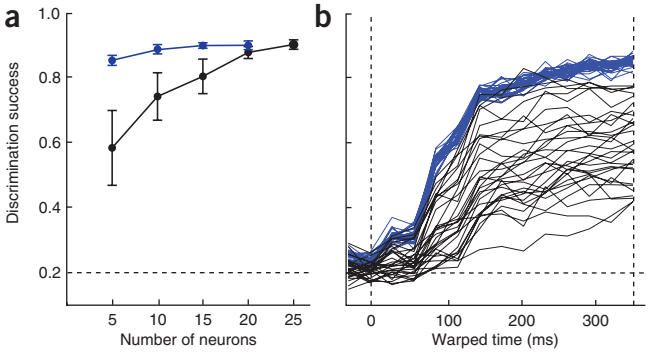

Figure 7 Discrimination among five odors by mitral/tufted cell populations. (**a**) Discrimination success as a function of number of neurons for 30-ms bin size. Dots are mean success over repeated permutations for random subsets (black dots) and the best subsets (blue dots). Error bars are s.d. (**b**) Discrimination performance of five-neuron ensembles as a function of sniff-warped time (30-ms bin). The black lines show individual permutations with random sets of five neurons and the blue lines show permutations with the best five neurons. The horizontal black dashed line marks chance level performance. Vertical dashed lines demarcate one sniff cycle.

DISCUSSION

To investigate olfactory information processing, we studied how sniffing shapes the odor responses of mitral/tufted cells in awake mice. We found that mitral/tufted cell odor responses exhibit very high temporal precision that has not been previously observed in the olfactory system. These precise responses tile the sniff cycle and lock to sniff phase rather than to latency from inhalation onset. In addition, the temporal patterns of responses carry copious information about stimulus at diverse timescales, such that a few cells may suffice to discriminate multiple stimuli.

Precision and diversity of odor responses

Although the precision that we observed has not been noted previously, temporal patterning relative to the sniff has been documented in previous work in anesthetized animals[7–9,21]. A recent study reported precision on the order of 20–40 ms and that relatively little information is carried in fine temporal structure[21]. However, anesthetized odor processing differs from awake processing in several important ways. Unanesthetized mitral/tufted cells have higher spontaneous activity[17], which indicates that the system is in a different state of excitability. Furthermore, anesthetized breathing is metronomic and stereotyped compared with awake breathing, which greatly alters the stimulus. These crucial differences in network state and stimulus sampling behavior may limit the utility of anesthetized preparations for understanding olfaction.

The temporal precision that we observed also surpasses that seen in previous studies in awake animals[20,22,23]. The primary reason for this difference is likely our use of a head-fixed, rather than a freely moving, configuration. Head fixation stabilizes the position of the nose relative to the odorant source, which ensures consistency of odor stimuli. The intensity of an odor stimulus can vary greatly with small differences in position relative to the odor output[24]. In addition, our method of sniff measurement, monitoring intranasal pressure, has been shown to preserve faster features of the sniff waveform more faithfully than thermocouple measurements[18]. Thus, by better controlling the stimulus, better measuring the animal's sampling behavior and by using a more sensible analysis, we discovered an unprecedented degree of temporal precision in odor coding.

Although olfaction is traditionally considered to be a 'slow' sense, the precision that we observed is comparable to that seen in other sensory modalities[3,4]. A further parallel with the visual system is that the precision of the neural representations becomes sharper as the timescale of stimulation becomes faster. For naturalistic movies, lateral geniculate nucleus neuronal responses have precision in the same range that we observed, whereas it approaches the 1-ms timescale for faster random flicker movies. Similarly, we found that mitral/tufted cells responded to odor more precisely for faster sniffs (**Fig. 5d**).

Information content in single and multi-unit activity

As a consequence of high temporal precision and reliability, a single cell's activity carries robust information about stimuli. This information was transmitted on different timescales, ranging from a few ms to the entire sniff cycle, as can be seen by the broad distribution of discrimination success rise times (**Fig. 6b**). Some cells transition from chance to highly accurate discrimination in a very short time interval ~10 ms. Across cells, these transitions occur at broad variety of latencies relative to the inhalation onset, consistent with the diversity of the odor response patterns.

The existence of individual neurons whose activity can discriminate two odors suggests that a small number of mitral/tufted cells can suffice for accurate classification of a larger number of odors. Indeed, with the activity of only 25 neurons, a classifier can discriminate among five odors with 91% accuracy. The activity of five neurons suffices for 84% accuracy. Such high performance with so few cells is in marked contrast with a recent study in freely moving rats[23]. For that study's dataset, classifier analysis required the activity of 232 neurons to achieve 90% performance. This difference in the number of cells needed for accurate discrimination is likely a result of the greater stimulus control that is possible in the head-fixed preparation.

Temporal encoding and decoding mechanisms

Our observations support the hypothesis that response timing can encode information about the odor stimulus. By what mechanisms might this encoding process work? At least some of the precision and diversity of response times may originate in olfactory sensory neurons (OSNs). Recent work suggests that OSN response kinetics can be quite fast and can vary across odor stimuli[25–27]. If OSN responses are insufficiently precise, the olfactory bulb circuit may be necessary to enforce the temporal precision that we observed. Inhibitory inputs from periglomerular and granule cells could work to sculpt precise firing events from more prolonged, jittery OSN input[28]. Mitral/tufted cells receive prominent sniff-entrained oscillatory input in the absence of odor[29–32], which may combine with stimulus-driven input to determine response timing[31,33,34].

Although our analysis quantifies the trial-to-trial timing precision of individual cells, the cell-to-cell timing relationships during individual sniffs may be more functionally relevant. What does the timing precision of individual cells tell us about the synchrony of cell ensembles? As presented above, 78 of 467 (17%) of cell-odor pairs responded with sharp firing events with a precision on the order of 10 ms. The reliability of sharp events was, on average, 0.68 and tended to be higher for more precise events (**Fig. 5c**). The latency distribution of these sharp events tiled the sniff cycle (range, 43–324 ms; **Fig. 4d**). Given this precision, reliability and sniff cycle tiling, we estimate that in each 10-ms window of a sniff in the presence of odor, a new ensemble comprising roughly 0.5% of mitral/tufted cells (approximately 250 cells in the mouse) will begin a sharp excitatory response. The timescale at which these mitral/tufted cell ensembles lock to the sniff rhythm matches the integration time window for coincidence detection of piriform cortical neurons[35,36].

Sniffing in awake animals is quite variable. We found that mitral/tufted cell response timing covaried with cycle-by-cycle variation in the sniff cycle, showing higher precision in sniff phase coordinates than in real time. This locking to sniff phase works to maintain synchrony relationships among mitral/tufted cells. Thus, sequential activation of synchronized assemblies of mitral/tufted cells will lead to excitation of the same population

of pyramidal cells independently of sniffing frequency, providing a basis for coding invariance relative to sniffing rhythm variability.

The organization of the bulb's projection to piriform cortex seems well suited to transmit such an ensemble code. Anatomical[37,38] and Ca^{2+} imaging[39] studies have suggested that mitral cells project diffusely and randomly to the piriform cortex. In this sense, the projection from bulb to cortex resembles the connection between the homologous structures in the insect: the antennal lobe and the mushroom body. In both systems, time-locked feed-forward inhibition defines a narrow integration window for principal neurons: piriform pyramidal cells in rodents[36] and mushroom body Kenyon cells in insects[40]. In locusts, numerous mechanisms stabilize the phase relationships of spiking in spite of frequency variability of local field potential oscillations[40–42]. Similar mechanisms may generate the sniff invariance that we found. These similarities between phylogenetically distant species suggest that synchronization of cell assemblies and coincidence detection is an evolutionarily conserved strategy for olfactory computation[6].

However, although our data are consistent with an ensemble coding hypothesis, the accurate discriminations achievable by individual neurons (**Fig. 6**) suggest that the activity of small numbers of neurons may suffice for perception[43]. In addition, although we found that neurons can transmit information on fast timescales, the rise time of discrimination can also be slow. Why does this information surplus exist? This likely reflects the simplicity of our stimulus set compared with what olfactory systems have evolved to solve. In natural olfactory scenes, individual odor sources can emit hundreds of chemical species, which propagate to the nose by turbulent airflow. Before we can begin to grapple with these complicated conditions, we must first establish a baseline with simplified stimuli under tight experimental control. In this way, our work facilitates studies that push olfaction closer to perceptual limits and/or naturalistic stimuli.

METHODS

Methods and any associated references are available in the online version of the paper at http://www.nature.com/natureneuroscience/.

Note: Supplementary information is available on the Nature Neuroscience website.

ACKNOWLEDGMENTS

We thank J. Osborne and T. Tabachnik for design and fabrication of experimental equipment, S. Royer for help with electrophysiological setup, J. Nunez-Iglesias for help with statistical analysis, P. Ahammad, D.B. Chklovskii and S. Druckmann for discussions and A. Resulaj, J.T. Dudman, V. Jayaraman, E. Pastalkova and K. Svoboda for comments on the manuscript. R.S., M.C.S. and D.R. are supported by the Howard Hughes Medical Institute. A.A.K. was supported by US National Institutes of Health grant R01 EY018068.

AUTHOR CONTRIBUTIONS

R.S. and D.R. conceived and designed the experiments. R.S., M.C.S. and D.R. performed experiments. R.S., A.A.K. and D.R. analyzed the data. R.S., M.C.S., A.A.K. and D.R. wrote the manuscript.

COMPETING FINANCIAL INTERESTS

The authors declare no competing financial interests.

Published online at http://www.nature.com/natureneuroscience/.
Reprints and permissions information is available online at http://www.nature.com/reprints/index.html.

1. Bair, W. & Koch, C. Temporal precision of spike trains in extrastriate cortex of the behaving macaque monkey. *Neural Comput.* **8**, 1185–1202 (1996).
2. Berry, M.J., Warland, D.K. & Meister, M. The structure and precision of retinal spike trains. *Proc. Natl. Acad. Sci. USA* **94**, 5411–5416 (1997).
3. Butts, D.A. *et al.* Temporal precision in the neural code and the timescales of natural vision. *Nature* **449**, 92–95 (2007).
4. Wehr, M. & Zador, A.M. Balanced inhibition underlies tuning and sharpens spike timing in auditory cortex. *Nature* **426**, 442–446 (2003).
5. Rieke, F., Warland, D., de Ruyter van Steveninck, R. & Bialek, W. *Spikes: Exploring the Neural Code* (MIT Press, Cambridge, Massachusetts, 1997).
6. Laurent, G. Olfactory network dynamics and the coding of multidimensional signals. *Nat. Rev. Neurosci.* **3**, 884–895 (2002).
7. Chaput, M.A. Respiratory-phase-related coding of olfactory information in the olfactory-bulb of awake freely breathing rabbits. *Physiol. Behav.* **36**, 319–324 (1986).
8. Fantana, A.L., Soucy, E.R. & Meister, M. Rat olfactory bulb mitral cells receive sparse glomerular inputs. *Neuron* **59**, 802–814 (2008).
9. Buonviso, N. *et al.* Rhythm sequence through the olfactory bulb layers during the time window of a respiratory cycle. *Eur. J. Neurosci.* **17**, 1811–1819 (2003).
10. Kepecs, A., Uchida, N. & Mainen, Z.F. The sniff as a unit of olfactory processing. *Chem. Senses* **31**, 167–179 (2006).
11. Abraham, N.M. *et al.* Maintaining accuracy at the expense of speed: stimulus similarity defines odor discrimination time in mice. *Neuron* **44**, 865–876 (2004).
12. Uchida, N. & Mainen, Z.F. Speed and accuracy of olfactory discrimination in the rat. *Nat. Neurosci.* **6**, 1224–1229 (2003).
13. Rinberg, D., Koulakov, A. & Gelperin, A. Speed-accuracy tradeoff in olfaction. *Neuron* **51**, 351–358 (2006).
14. Doucette, W. & Restrepo, D. Profound context-dependent plasticity of mitral cell responses in olfactory bulb. *PLoS Biol.* **6**, e258 (2008).
15. Fuentes, R.A., Aguilar, M.I., Aylwin, M.L. & Maldonado, P.E. Neuronal activity of mitral-tufted cells in awake rats during passive and active odorant stimulation. *J. Neurophysiol.* **100**, 422–430 (2008).
16. Kay, L.M. & Laurent, G. Odor- and context-dependent modulation of mitral cell activity in behaving rats. *Nat. Neurosci.* **2**, 1003–1009 (1999).
17. Rinberg, D., Koulakov, A. & Gelperin, A. Sparse odor coding in awake behaving mice. *J. Neurosci.* **26**, 8857–8865 (2006).
18. Verhagen, J.V., Wesson, D.W., Netoff, T.I., White, J.A. & Wachowiak, M. Sniffing controls an adaptive filter of sensory input to the olfactory bulb. *Nat. Neurosci.* **10**, 631–639 (2007).
19. Laurent, G., Wehr, M. & Davidowitz, H. Temporal representations of odors in an olfactory network. *J. Neurosci.* **16**, 3837–3847 (1996).
20. Pager, J. Respiration and olfactory-bulb unit-activity in the unrestrained rat: statements and reappraisals. *Behav. Brain Res.* **16**, 81–94 (1985).
21. Bathellier, B., Buhl, D.L., Accolla, R. & Carleton, A. Dynamic ensemble odor coding in the mammalian olfactory bulb: sensory information at different timescales. *Neuron* **57**, 586–598 (2008).
22. Bhalla, U.S. & Bower, J.M. Multiday recordings from olfactory bulb neurons in awake freely moving rats: spatially and temporally organized variability in odorant response properties. *J. Comput. Neurosci.* **4**, 221–256 (1997).
23. Cury, K.M. & Uchida, N. Robust odor coding via inhalation-coupled transient activity in the mammalian olfactory bulb. *Neuron* **68**, 570–585 (2010).
24. Vetter, R.S., Sage, A.E., Justus, K.A., Carde, R.T. & Galizia, C.G. Temporal integrity of an airborne odor stimulus is greatly affected by physical aspects of the odor delivery system. *Chem. Senses* **31**, 359–369 (2006).
25. Raman, B., Joseph, J., Tang, J. & Stopfer, M. Temporally diverse firing patterns in olfactory receptor neurons underlie spatiotemporal neural codes for odors. *J. Neurosci.* **30**, 1994–2006 (2010).
26. Nagel, K.I. & Wilson, R.I. Biophysical mechanisms underlying olfactory receptor neuron dynamics. *Nat. Neurosci.* **14**, 208–216 (2011).
27. Spors, H., Wachowiak, M., Cohen, L.B. & Friedrich, R.W. Temporal dynamics and latency patterns of receptor neuron input to the olfactory bulb. *J. Neurosci.* **26**, 1247–1259 (2006).
28. Shepherd, G.M. ed. *The Synaptic Organization of the Brain* (Oxford University Press, 2004).
29. Adrian, E.D. The electrical activity of the mammalian olfactory bulb. *Electroencephalogr. Clin. Neurophysiol.* **2**, 377–388 (1950).
30. Sobel, E.C. & Tank, D.W. Timing of odor stimulation does not alter patterning of olfactory-bulb unit-activity in freely breathing rats. *J. Neurophysiol.* **69**, 1331–1337 (1993).
31. Margrie, T.W. & Schaefer, A.T. Theta oscillation coupled spike latencies yield computational vigor in a mammalian sensory system. *J. Physiol. (Lond.)* **546**, 363–374 (2003).
32. Cang, J. & Isaacson, J.S. In vivo whole-cell recording of odor-evoked synaptic transmission in the rat olfactory bulb. *J. Neurosci.* **23**, 4108–4116 (2003).
33. Hopfield, J.J. Pattern-recognition computation using action-potential timing for stimulus representation. *Nature* **376**, 33–36 (1995).
34. Brody, C.D. & Hopfield, J.J. Simple networks for spike-timing-based computation, with application to olfactory processing. *Neuron* **37**, 843–852 (2003).
35. Franks, K.M. & Isaacson, J.S. Strong single-fiber sensory inputs to olfactory cortex: Implications for olfactory coding. *Neuron* **49**, 357–363 (2006).
36. Poo, C. & Isaacson, J.S. Odor representations in olfactory cortex: 'sparse' coding, global inhibition, and oscillations. *Neuron* **62**, 850–861 (2009).
37. Haberly, L.B. & Price, J.L. Axonal projection patterns of mitral and tufted cells of olfactory-bulb in rat. *Brain Res.* **129**, 152–157 (1977).
38. Miyamichi, K. *et al.* Cortical representations of olfactory input by trans-synaptic tracing. *Nature* **472**, 191–196 (2011).
39. Stettler, D.D. & Axel, R. Representations of odor in the piriform cortex. *Neuron* **63**, 854–864 (2009).
40. Perez-Orive, J. *et al.* Oscillations and sparsening of odor representations in the mushroom body. *Science* **297**, 359–365 (2002).
41. Cassenaer, S. & Laurent, G. Hebbian STDP in mushroom bodies facilitates the synchronous flow of olfactory information in locusts. *Nature* **448**, 709–713 (2007).
42. Assisi, C., Stopfer, M., Laurent, G. & Bazhenov, M. Adaptive regulation of sparseness by feedforward inhibition. *Nat. Neurosci.* **10**, 1176–1184 (2007).
43. Barlow, H.B. Single units and sensation: a neuron doctrine for perceptual psychology? *Perception* **1**, 371–394 (1972).

ONLINE METHODS

Animals. Data were collected in four C57BL/6J mice and three OMP-ChannelRhodopsin-YFP heterozygous mice that had a targeted insertion in the OMP locus (data not shown). All mice had at least one normal copy of *Omp*. No differences were observed between these two groups of mice. Subjects were 6–8 weeks old at the beginning of behavioral training and were maintained on a 12-h light/dark cycle (lights on at 8:00 p.m.) in isolated cages in a temperature- and humidity-controlled animal facility. All animal care and experimental procedures were in strict accordance with a protocol approved by the Howard Hughes Medical Institute Institutional Animal Care and Use Committee.

Electrophysiology. Mitral/tufted cell spiking activity was recorded using 16- or 32-channel Si-probes (NeuroNexus, model: a2x2-tet-3mm-150-150-312(F16), a4x8-5mm-150-200-312(F32)) or home-made microdrive with 16 individually adjustable 3 MOhm PtIr electrodes. Cells were recorded in both ventral and dorsal mitral cell layers. The identity of mitral/tufted cells were established on the basis of criteria formulated in previous work[17]. The data were acquired using a 32-channel data acquisition system (Digital Lynx, NeuraLynx) with widely open broadband filters and sampling frequency of 0.1–9,000 Hz.

Sniff recording. To monitor the sniff signal, we implanted a thin 7-mm-long stainless cannula (gauge 23, Small Parts capillary tubing) in the nasal cavity. The cannula was capped between experimental recordings. During experiments, the cannula was connected to a pressure sensor with polyethylene tubing (801000, A-M Systems). The pressure was measured with pressure sensor (MPX5050, Freescale Semiconductor) and homemade preamplifier circuit. The signal from the preamplifier was recorded together with electrophysiological data on one of the data acquisition channels. The timing of the pressure signal was calibrated against the hot wire anemometer (mini CTA 5439, Dantec Dynamics, Denmark) and shifted back for 32 ms for all analysis (**Supplementary Note** and **Supplementary Fig. 1**).

Surgery. Mice were anesthetized using isofluorane gas anesthesia. The horizontal bar for head fixation, pressure cannula and electrode chamber were implanted during a single surgery. To implant the sniffing cannula, a small hole was drilled in the nasal bone, into which the cannula was inserted and affixed with glue and stabilized with dental cement. To implant the electrode chamber, a small craniotomy (~1 mm^2) was done above left or right olfactory bulb. After the insertion of the Si-probe/electrodes, the electrode chamber was fixed by dental cement to the skull, posterior to the olfactory bulb. The reference electrode was implanted in cerebellum. The mice were given at least 5 d after a surgery for recovery.

Behavioral procedure and training. After recovery, the mice were placed in the head-fixation setup. The first few sessions were brief (10–20 min) and served to acclimate the animals to head fixation in the setup. Mice typically remained mostly quiescent after 1–2 sessions of head fixation, after which odor sessions started. We delivered 1 of 2–10 odors in pseudo-random sequence with an average interstimulus interval of 6 s and stimulus duration of 500–1,000 ms. During early experiments, odor was delivered randomly with respect to the sniff cycle. When we noticed the precise sniff timing of neuronal responses, we started triggering odor delivery, that is, final valve opening (see next section), on the beginning of the exhalation phase, which was detected by positive-going zero crossings of the pressure signal. This prevents odor from being delivered at random times during inhalation, which would confound our analysis. Furthermore, as no odor enters the nose during exhalation phase, this allows enough time for the odor stimulus to reach a steady state of concentration by the time the animal begins inhaling. One session usually lasted for 30–60 min and contained 300–400 trails.

Odor delivery. For stimulus delivery we used a nine-odor air dilution olfactometer. The air flow through the selected odorant vial was diluted ten times by the main airflow stream and homogenized in a long thin capillary before reaching the final valve. It took approximately 500–1,000 ms to prepare the homogenized mixture and equilibrate the concentration. A steady stream of 1,000 ml min^{-1} of clean air was flowing to the odor port all of the time except during stimulus delivery, when the flow from the olfactometer was directed to an exhaust. After sufficient mixing and equilibration time, the final valve (four-way Teflon valve, NResearch) switched the odor flow to the odor port, and diverted the clean airflow to the exhaust. All flows and line impedances were tuned to minimize the pressure shock resulting from line switching and minimize the time of odor concentration stabilization after opening the final valve. Temporal odor concentration profile was checked by mini-PID (Aurora Scientific). The concentration reached a steady state 25–40 ms after final valve opening.

We used multiple odorants obtained from Sigma-Aldrich. The odorants were stored in liquid phase (diluted 1:5 in mineral oil) in dark vials. The odorant concentration delivered to the animal was reduced an additional tenfold by air dilution. We used acetophenone, amyl acetate, behzaldehyde, butyric acid, decanol, ethyl acetate, ethyl tiglate, 1-hexanol, hexanoic acid, hexanal, 2-hexanone, hexyl acetate, R-limonene, isopropyl tiglate, methyl benzoate, methyl salicylate, 1-octanol and 2-undecanone as odorants. All of the analysis discussed below was done in Matlab (MathWorks).

Spike extraction. Acquired electrophysiological data were filtered and spike sorted. For Si-probe data we used MClust software package (A.D. Redish) and software package written by A.A.K. PtIr electrode data was not sorted and a simple threshold crossing spike detection criteria was used to extract spike times.

Temporal warping. Sniffing recordings were down-sampled to 1 kHz, and filtered in the range of 0.5–20 Hz. Initially, the times of inhalation onset and offset were detected by negative and positive zero-crossings, respectively. Often the positive zero-crossing at the end of inhalation phase was not well defined, owing to the very shallow slope of the signal. To more reliably estimate the offset of the inhalation phase, we fit a parabola to the minima of the pressure signal following the onset of the inhalation (**Fig. 1b**). Inhalation offset was defined as the second zero crossing of the parabola. We defined two intervals: the first is from inhalation onset to inhalation offset and the second is the rest of the sniffing cycle, from the inhalation offset to the next inhalation onset. For the whole session, we estimated an average duration for both intervals. Each interval of the sniffing data, together with correspondent spiking data, was stretched or compressed to make its duration equal to the duration of the average interval.

Odor responses. We compared the distributions of the neuronal activity with and without odors. Distribution without stimulus was sampled from five sniffs preceding the odor delivery across all trials (approximately 1,500–2,000 sniffs for each session). Distribution of neuronal responses for a given odor was sampled from the first sniff after stimulus onset for the trials containing a correspondent odor delivery. Latencies of odor responses were estimated as the first time point when the cumulative distribution of the number of spikes from the inhalation onset was significantly different for background and stimulus distributions (Kolmogorov-Smirnov test, $P < 0.004$, corresponding to a false discovery rate of 0.05 using the Benjamini-Hochberg multiple testing correction). The cumulative distributions were calculated using spike times binned at 1 ms. The response was consider to be excitatory or inhibitory if the first deviation from the background distribution was positive or negative, respectively. For estimation of the responses based on the whole sniff spike count, we compared the total number of spike in sniffs with and without stimulus (Kolmogorov-Smirnov test, $P < 0.009$, corresponding to a false discovery rate of 0.05 using the Benjamini-Hochberg multiple testing correction). For estimation multimodal responses the distributions of number of spikes at each sequential 10-ms bin for odorized and not-odorized sniffs were compared (Kolmogorov-Smirnov test, $P < 0.01$, corresponding to a false discovery rate of 0.05 using the Benjamini-Hochberg multiple testing correction).

Precision estimation. To estimate precision, we used a previously proposed method[1]. First, we found events of sharp firing rate increase based on the peak of the PSTH calculated using 10-ms bins. If the amplitude of the PSTH in presence of stimulus was at least twice as high as the averaged firing rate in pre-stimulus sniffing cycle, this response was chosen for precision analysis. We searched for the occurrence of the spikes with an interspike interval shorter than 1.5/(PSTH peak amplitude) in the temporal vicinity of the peak (from −2 to +4 interspike interval) (**Fig. 4**). The precision was defined as a jitter of the first spike (green circle) across trials. The reliability was defined as a portion of trials when such spikes exist.

Information content estimation. To quantify information content we used the TMA procedure[21]. For the case of single neurons (**Fig. 6**), we used 5-ms bins starting 200 ms before inhalation onset. The calculation was based on 1,734 cell-odor combinations. For every cell and for every pair of odorants we counted spikes in time bins for every trial. For every trial, we built a set of templates that defined average spike counts produced by this cell to each of the included odorants $\bar{r}_{OT}$. Here, the indices O and T denote odorant and time bin. The averaging excluded data in the given trial. The spike counts in the given trial r_T were then compared with $\bar{r}_{OT}$ and the nearest vector $\bar{\mathbf{r}}_O$ specified the guess for the odorant O presented in the trial on the basis of mitral cell activity. This guess was then compared with the odorant actually presented to yield the estimate for discrimination success. We increased the length of vector $\mathbf{r}_T$ to include progressively larger concatenated set of bins to yield discrimination success as a function of time $c(t)$. $c(t)$ was fitted with a sigmoid function $c(t)=p_1+p_2(\tanh(2(t-\tau)/\delta)+1)/2$. Here the parameters p_1, p_2, τ and δ represent the asymptotic values of success rate, response latency and response width (**Fig. 6a**). The maximum correct rate (**Fig. 6b**) was defined by $D=p_1+p_2$. We chose 886 pairs with significant increase in the discrimination success rate by performing right-tailed t test on the values of p_2 obtained from fitting the bootstrapped values of $c(t)$ resampled from different trials with repetitions (**Fig. 6b**,**c**). 300 iterations of bootstrap were used. 886 odor-odor-cell triples were included out of 1,734 on the basis of false discovery rate of 0.01 (**Fig. 6b**,**c**). For population analysis, we used a similar TMA procedure. In this case the response vector $\mathbf{r}_{TN}$ and the template $\bar{r}_{OTN}$ included the additional set of indices N describing the neuron for which given response is obtained. The guess for odorant O was found in individual trials from the identity of the template $\bar{r}_{OTN}$ that is most similar to the response vector $\mathbf{r}_{TN}$. The classification success was determined by comparing this guess with the odorant actually presented. Because neurons were not recorded simultaneously, trials corresponding to different neurons were assembled from the data randomly. For multi-neuronal analysis we increased the bin size from 5 to 30 ms to avoid undersampling problems arising from larger number of dimensions[44].

44. Bishop, C. *Pattern Recognition and Machine Learning* (Springer, 2006).

doi:10.1038/nn.2877